TISSUE ENGINEERING: Part C
Volume 22, Number 11, 2016

DOI: 10.1089/ten.tec.2016.0261

termis
Tissue Engineering
& Regenerative Medicine
International Society

*METHODS ARTICLE*

# Establishing Proximal and Distal Regional Identities in Murine and Human Tissue-Engineered Lung and Trachea

Andrew Trecartin, MD,[1,2] Soula Danopoulos, PhD,[1,2] Ryan Spurrier, MD,[1,2] Hanaa Knaneh-Monem, MSc,[2,3] Michael Hiatt, PhD,[2] Barbara Driscoll, PhD,[2] Christian Hochstim, MD, PhD,[2–4] Denise Al-Alam, PhD,[1,2,4] and Tracy C. Grikscheit, MD[1,2,4]

The cellular and molecular mechanisms that underpin regeneration of the human lung are unknown, and the study of lung repair has been impeded by the necessity for reductionist models that may exclude key components. We hypothesized that multicellular epithelial and mesenchymal cell clusters or lung organoid units (LuOU) could be transplanted to recapitulate proximal and distal cellular structures of the native lung and airways. Transplantation of LuOU resulted in the growth of tissue-engineered lung (TELu) that contained the necessary cell types consistent with native adult lung tissue and demonstrated proliferative cells at 2 and 4 weeks. This technique recapitulated important elements of both mouse and human lungs featuring key components of both the proximal and distal lung regions. When LuOU were generated from whole lung, TELu contained key epithelial and mesenchymal cell types, and the origin of the cells was traced from both $Actin^{GFP}$ and $SPC^{GFP}$ donors to indicate that the cells in TELu were derived from the transplanted LuOU. Alveolar epithelial type 2 cells (AEC2s), club cells, ciliated cells marked by beta-tubulin IV, alveolar epithelial type I cells, Sox-2-positive proximal airway progenitors, p63-positive basal cells, and CGRP-positive pulmonary neuroendocrine cells were identified in the TELu. The mesenchymal components of peribronchial smooth muscle and nerve were identified with a CD31-positive donor endothelial cell contribution to TELu vasculature. TELu successfully grew from postnatal tissues from whole murine and human lung, distal murine lung, as well as murine and human trachea. These data support a model of postnatal lung regeneration containing the diverse cell types present in the entirety of the respiratory tract.

**Keywords:** adult stem cells, lung, trachea, tissue engineering, human, mouse

## Introduction

Lung disease is mortal, with over 230,000 annual deaths in the United States, and damaged lung epithelium often responds to injury and disease with scarring rather than repair, the mechanisms of which are not well understood.[1–3] Postnatal lung regeneration in human patients occurs in a complex system influenced by three-dimensional relationships between diverse cell types and environmental cues. However, conventional reductionist models are limited in ways that may limit translation: two-dimensional systems, isolated cell types, poor viability on decellularized scaffolds, or embryonic-like tissues may be too different from the relative complexity of *in vivo* native lung.[4] Although the lung is, in general, relatively quiescent, it does respond to injury with regenerative processes we do not currently understand. Study of these models has been limited by two factors: the difficulty of maintaining *in vivo* experiments such as recellularized tissues beyond short-term limits and the immaturity of induced pluripotent stem cell-differentiated cell products that do not yet model fully mature postnatal lung tissue.[5,6] Alveolar epithelial cells seeded onto decellularized lung matrices show a rapid decrease in epithelial markers and increase in mesenchymal cells within only a few days, which is not enough time to effectively model regeneration.[7]

Our laboratory has successfully generated functional tissue-engineered intestine that demonstrates all of the key components of native tissue from both human and murine postnatal donor tissue on biodegradable polymer scaffolds.[8,9] And so,

[1]Division of Pediatric Surgery, Children's Hospital Los Angeles, Los Angeles, California.
[2]Developmental Biology and Regenerative Medicine Program, Saban Research Institute, Children's Hospital Los Angeles, Los Angeles, California.
[3]Division of Otolaryngology, Children's Hospital Los Angeles, Los Angeles, California.
[4]Keck School of Medicine, University of Southern California, Los Angeles, California.

we hypothesized that we could optimize this method to allow various regions of the mouse and human lung and airway to develop *in vivo* as tissue-engineered lung (TELu) to establish a more complete system, in which the various primary cell types of proximal and distal lung may proliferate for eventual understanding of lung regeneration. TELu formed efficiently from mouse and human tissue, demonstrated regional cell types on further refining the source selection of the donor lung organoid units (LuOU), and cells in the TELu proliferated at 2 and 4 weeks *in vivo*. Generation of these constructs from mouse and human tissues may allow us in future work to dissect the cellular and molecular mechanisms of *in vivo* lung regeneration and repair that are required for human survival of lung disease.

## Materials and Methods

### *LuOU preparation*

All animals were cared for according to our Institutional Animal Care and Use Committee-approved protocol. Human tissue from normal margins of lung resections performed at our children's hospital was submitted to us after consultation with the institutional review board as deidentified tissue, without any accompanying patient identifiers. LuOU were generated similar to our previously described protocol for intestine[9] starting with either whole lung, proximal airway excised from between the larynx and the main stem bronchi, or distal airway consisting of a 3 mm edge resection from each lung lobe. Briefly, lung tissue from C57BL/Ka-beta-actin-EGFP ($Actin^{GFP}$) mice (gift from Dr. Wagers, Harvard Stem Cell Institute) between 2 and 3 weeks old, $SPC^{GFP}$ mice[10] the same age, or from deidentified human lung resections was minced into pieces smaller than 1 mm in diameter, washed with HBSS (14170-112; Thermo Fisher) supplemented with 1% Anti-Anti (15240062; Thermo Fisher) (HBSS+Anti-Anti), and centrifuged at 150 *g* for 1 min. The wash was repeated and the supernatant decanted.

Tissue was then incubated in 10 mL of HBSS+Anti-Anti supplemented with collagenase type IV (LS004188; Worthington) at 1110 and 2 U/mL Dispase (17105041; Thermo Fisher) at 37°C for 20 min. The enzymatic reaction was stopped by adding 2 mL of Dulbecco's modified Eagle's medium (DMEM) (11965-092; Thermo Fisher) supplemented with 10% fetal bovine serum (FBS) and 1% Anti-Anti (10%FBS/DMEM+Anti-Anti). The tissue was triturated by pipetting the solution 50 times with a 10-mL serological pipette.

The solution was centrifuged at 150 *g* for 1 min, the supernatant was removed, and the tissue pellet washed with 10% FBS/DMEM+Anti-Anti, centrifuged, and the supernatant discarded. No more solution was added. This resulted in multicellular clusters termed LuOU that were ready for loading onto scaffolds. Scaffolds were prepared according to our previously published protocol, composed of polyglycolic acid coated with poly-L-lactic acid and type I collagen.[9] The cylindrical scaffolds were cut to be 3–4 mm long and the outside of the scaffold was coated with 60 μL of LuOU.

### *Surgical implantation*

Nonobese diabetic severe combined immunodeficiency interleukin (IL)-2 gamma light chain-deficient (NSG) mice (Stock No: 005557; Jackson Laboratories) received 350 cGy radiation before the procedure on the day of surgery. They were subsequently anesthetized with isoflurane and received subcutaneous injection of ketoprofen (2 mg/kg). The abdomen was prepped, draped, and 3–4 mm incisions were made in the midline followed by lateral dissection to create a narrow subcutaneous tract to the lateral abdomen/flank. Scaffold loaded with LuOU was inserted to lie at the end of the tract. Each NSG mouse received 1–6 implants with each implant being inserted into an individual subcutaneous pocket. The incisions were closed with 4-0 Vicryl sutures. Mice received Ibuprofen suspension (Perrigo®) at 20 mg per 100 mL drinking water for the first 3 postoperative days and Septra 200 mg/40 mg per 5 mL (Hi-Tech Pharmacal) at 1:100 dilution in their drinking water for their entire course. Four weeks after insertion, the implants were harvested as TELu and placed in formalin followed by paraffin embedding.

### *Immunofluorescence*

Following embedding, tissues were sectioned at 5 μm thickness. Sections were cleared twice in Histochoice and rehydrated in graded ethanol solutions. Slides were washed in phosphate-buffered saline (PBS) and underwent antigen retrieval in low pH sodium citrate buffer (Vector) with a BioCare Decloaking Chamber heated to 125°C followed by cooling to 90°C. The slides were then cooled for 20 min and washed in PBS. They were then blocked in a solution containing 2% goat serum, 1% bovine serum albumin (BSA), 0.1% cold fish skin gelatin, 0.1% Triton X-100, and 0.05% Tween® 20 (Sigma) in 0.01 M PBS. If donkey secondary antibodies were used, then 2% donkey serum was substituted for goat serum. The beta-tubulin IV antibody was incubated in 3% BSA with 0.4% Triton. The rest of the primary antibodies (Supplementary Table S1; Supplementary Data are available online at www.liebertpub.com/tec) were diluted in 1% BSA, 0.1% cold fish skin gelatin, and 0.5% Triton X-100 in PBS. Tissue sections were incubated with the primary antibodies at 4°C overnight. Slides were washed with 0.1% Tween 20 in PBS (PBS-T) and then incubated with secondary antibodies for 1 h at room temperature. After incubation with secondary antibodies, slides were washed in PBS-T, incubated with DAPI 1:500 in $dH_2O$ 5 min, and then washed in PBS for 5 min. Slides were mounted in Prolong Gold® and imaged with a Leica DMI6000 B inverted microscope.

### *Bromodeoxyuridine labeling*

Mice hosting TELu implants received an intraperitoneal (IP) injection of bromodeoxyuridine (BrdU) at specified time points in four separate groups. To evaluate early time points, there were two groups: one received BrdU 100 mg/kg 1 week postimplant and harvested 1 week later (2 weeks postimplant). A second early group received BrdU 100 mg/kg at the time of surgical implant and TELu was harvested at 1 week postimplant. To evaluate later time points, a third group received BrdU injection 2 g per mouse 24 h before harvest at 4 weeks, and a fourth group received BrdU 100 mg/kg 2 weeks postimplant and harvested 2 weeks later (4 weeks postimplant). Host native lung and intestine served as additional control specimens due to the rapid epithelial turnover of the intestine.

*Cell quantification*

Slides from four different animals with implantations were stained with P63 (basal cells), CC10 (club cells), or BrdU injected 24 h before harvest at 4 weeks (proliferation). Each slide was then imaged at 40× magnification, with a minimum of three images taken per slide (an average of five images were taken of most slides). For P63 and CC10, the epithelial cells were counted within the frame comparing positive cells to the total number of proximal epithelial cells. These numbers were then averaged and reported as a percentage.

A similar process was followed with BrdU staining. Slides from five different animals with implantations were stained with BrdU. Counting was performed for both total TELu and proximal epithelial structures and reported as percentage of total BrdU-positive cells compared to the total cell number as well as total positive proximal epithelial BrdU cells compared to total proximal epithelium. Data were analyzed with Student's unpaired *t*-test in GraphPad Prism software (GraphPad).

## Results

Murine tissue-engineered lung (mTELu) was consistently generated. LuOU were generated from whole lung and transplanted in multiple sites subcutaneously on biodegradable scaffolds. After 4 weeks, the resulting mTELu was harvested. As we have noted in the transplantation of LuOU generated from the intestine in previous work, the polymer scaffold biodegrades and the resulting tissue-engineered structure replaces the biomaterial with growing cells (Fig. 1A). The efficiency of mTELu generation was determined from an initial cohort of mice that received a total of 32 implants, on average 4 implants per mouse. All 32 implants were confirmed to contain CC10-positive airway structures, indicating a 100% success rate of growth of mTELu. Throughout the course of subsequent experiments reported here, mTELu continued to generate CC10-positive airway structures and additional cell types were noted.

mTELu, when generated from whole lung tissue, contained both proximal and distal lung epithelial cells. TELu or tissue-engineered trachea (TEtrach) always reflected the cellular identity of the donor tissue. For example, implantation of human tracheal donor cells alone (Supplementary Fig. S1A, B) results only in the growth of tracheal components, whereas mixed populations of whole lung result in the growth of TELu containing both proximal and distal cells (Supplementary 1C–F).

On cross section, the mTELu implants contained numerous epithelial and mesenchymal cells consistent with those of native lung. LuOU from $SPC^{GFP}$ donor tissue generated mTELu containing donor GFP-positive cells (Fig. 1C) that were also positive for SPC (Fig. 1E), consistent with alveolar epithelial type 2 cells (AEC2s) (Fig. 1B–E). In addition to AEC2s, mTELu contained proximal airways lined by CC10-positive club cells; when generated from actin-GFP LuOU, these were confirmed to be of donor origin (Fig. 1F, G) and SPC-positive cells surrounded the CC10-positive structures (Fig. 1H, I). As previously noted in tissue-engineered intestine,[11,12] shed cells contribute to luminal contents, and CC10-positive debris are often seen in TELu proximal airway structures (Figs. 1I, 3F, and 4D) as would be expected from a club cell secretory protein.[13] mTELu generated from whole lung isolates also contained distal alveolar epithelial type I cells (AEC1s) identified by T1-alpha staining in proximity to AEC2s (Fig. 1K) comparable to native lung (Fig. 1J). When TELu was generated from $Actin^{GFP}$ mice, these AEC2s were double positive for GFP and SPC, indicating that these cells are of donor origin (Fig. 1L, M).

When generated from whole lung, key proximal components were identified. Characterization of the mTELu indicated the presence of proximal epithelial cell markers similar to the native lung. Goblet cells were identified by Alcian blue staining (Fig. 2A, B). Sox-2-positive proximal airway progenitors,[14] CGRP-positive pulmonary neuroendocrine cells, and p63-positive basal cells were also identified in TELu (Fig. 2C–H). p63 was not detected in native lung, but 22.5% ± 2.6% of cells in the proximal epithelium of TELu stained positive for p63 ($p = 0.0074$) (Fig. 2I). Ciliated cells were also present in mTELu as shown by beta-tubulin IV staining (Fig. 2K, N) and were interspersed between club cells (Fig. 2K) as in native lung (Fig. 2J, M). CC10 was not increased in TELu at 22.21% ± 2.11% of proximal epithelial cells for native lung and 31.02% ± 4.27% for TeLu ($p = 0.2218$) (Fig. 2L).

mTELu contains smooth muscle, vasculature, and nerves. In native lung, peribronchial smooth muscle cells line the proximal airways as shown by alpha-SMA staining (Fig. 3A, C). Similarly, in mTELu, peribronchial smooth muscle cells were present around proximal airway structures as confirmed by alpha-SMA staining (Fig. 3B, D). Costaining with GFP and CD31 identified a donor endothelial cell contribution to mTELu vasculature (Fig. 3C, D). Tuj1-positive peribronchial nerves were also identified in TELu comparable (Fig. 3F) to native lung (Fig. 3E).

There is evidence of cell proliferation in mTELu at 2 and 4 weeks postimplantation. Comparison of the native lungs with subcutaneously hosted mTELu demonstrated BrdU uptake in mTELu, but not in native lung (Fig. 4A, B) at time points of 2 weeks and beyond, but not at early time points. In hosts injected with BrdU 2 weeks before mTELu harvest (Fig. 4C–F), there was demonstrated BrdU uptake in both host native lung and mTELu in proximal and distal lung indicated by BrdU-positive staining in CC10-positive epithelium and SPC-positive AEC2s. In mice injected with BrdU 24 h before a 4-week harvest (Fig. 4A, B, G), greater numbers of BrdU cells were identified compared to native lung both in total TELu and in proximal epithelial structures formed in TELu. BrdU was significantly increased in TELu structures in all compartments combined (proximal epithelium, distal epithelium, and mesenchyme) (8.31 ± 1.24 vs. 0.82 ± 0.82, $p = 0.017$). Quantification of in proximal epithelium only of TELu showed a significant increase compared to proximal epithelium of native lung (4.54 ± 0.82 vs. 0.52 ± 0.52, $p = 0.034$).

Mice that received BrdU at the two early time points of implantation ($n = 3$ hosts) and 1 week after implantation ($n = 3$ hosts) did not demonstrate BrdU uptake in mTELu or host native lungs (data not shown), consistent with our previous findings in tissue-engineered intestine[9] where peak proliferation begins around 2 weeks. BrdU uptake was confirmed by staining the intestine of the host after harvest at 24-h post-BrdU IP injection, since the intestine is a rapidly cycling tissue.

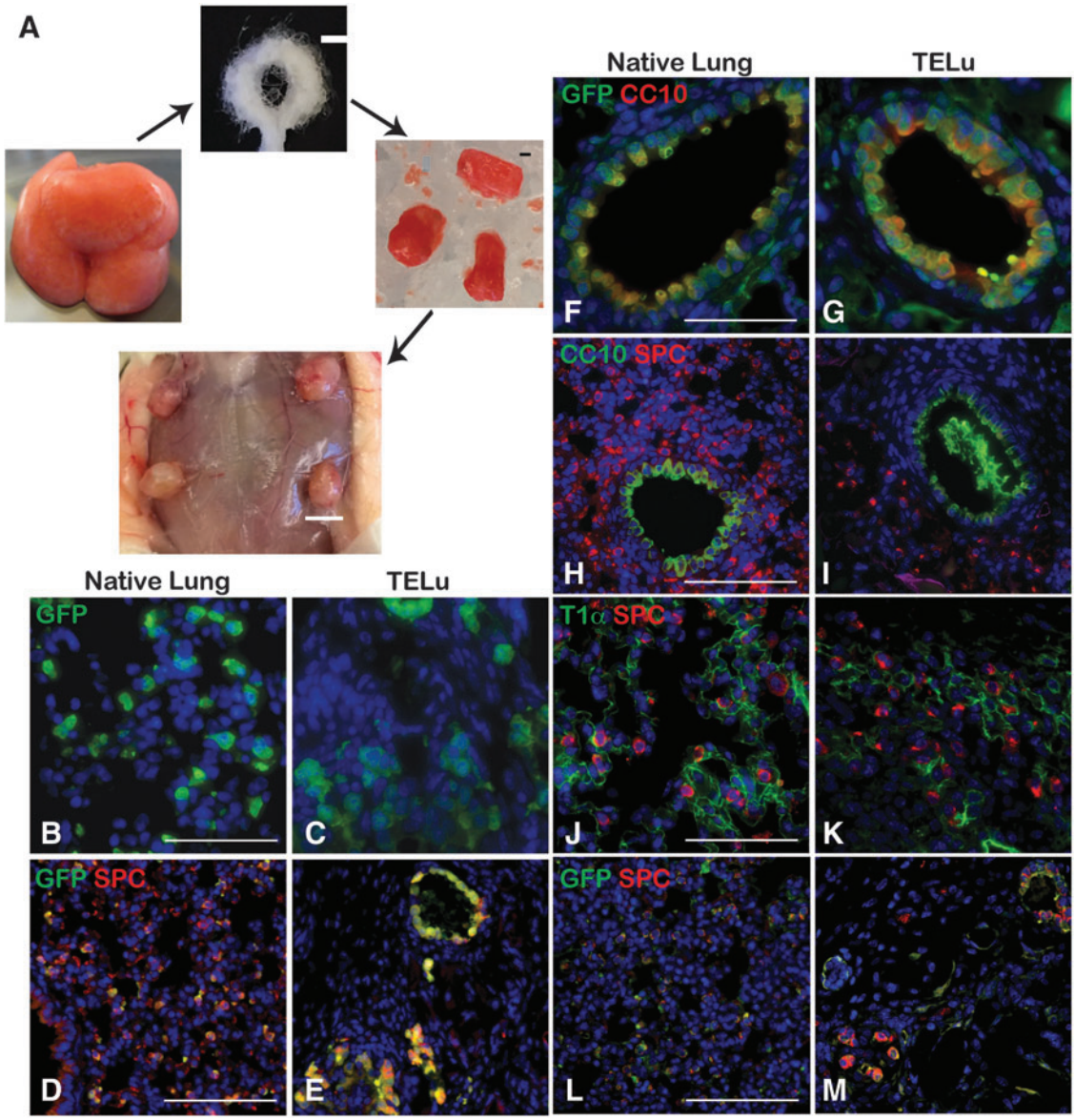


**FIG. 1.** LuOU are multicellular clusters derived from whole lung tissue **(A**, *left*). Polyglycolic acid and poly-L-lactic acid scaffolds **(A**, *top*) are loaded with LuOU **(A**, *right*), scale bar represents 1 mm. The loaded scaffolds are implanted subcutaneously into NSG hosts, where they remain 4 weeks before harvest as TELu **(A**, *bottom*), scale bar 5 mm. **(B, C)** IF staining for GFP (*green*) of $SPC^{GFP}$ native lung **(B)** and TELu generated from $SPC^{GFP}$ lung **(C)**, scale bar 50 µm. **(D, E)** IF staining for GFP (*green*) and SPC (*red*), expressed by AEC2s, on $SPC^{GFP}$ native lung **(D)** and TELu **(E)** generated from $SPC^{GFP}$ lung, scale bar 100 µm. **(F, G)** IF for CC10 (*red*) to mark proximal airway club cells and GFP (*green*) in $Actin^{GFP}$ native lung **(F)** and TELu **(G)** generated from $Actin^{GFP}$ donor tissue ($Actin^{GFP}$ TELu), scale bar 50 µm. **(H, I)** IF for CC10 (*green*) and SPC (*red*) for $Actin^{GFP}$ native lung **(H)** and $Actin^{GFP}$ TELu **(I)**, scale bar 50 µm. **(J, K)** IF for T1α (AEC1s) (*green*) and SPC (*red*) in native lung **(J)** and TELu **(K)**, scale bar 50 µm. **(L, M)** IF for GFP (*green*) and SPC (*red*) in $Actin^{GFP}$ native lung **(L)** and $Actin^{GFP}$ TELu, scale bar 100 µm. IF, immunofluorescent; LuOU, lung organoid unit; TELu, tissue-engineered lung. Color images available online at www.liebertpub.com/tec

Human TELu was successfully generated from postnatal human lung tissue. AEC2s were identified in human tissue-engineered lung (hTELu) as evidenced by SPC staining (Fig. 5A, B). Airways in native lung and hTELu were lined with alpha-SMA-positive smooth muscle cells (Fig. 5C, D), confirmed to be of human origin by costaining for human-specific beta-2-microglobulin. hTELu demonstrated numerous E-cadherin-lined airway structures deriving from the human LuOU as they are also positive for human-specific beta-2-microglobulin (Fig. 5E, F).

Isolated regionally specific proximal and distal LuOU generated tissue-engineered structures that conserve the characteristics of their origin, including appropriate epithelial cell types. Once we had determined that TELu could be generated from murine and human tissue, we sought to create regionally specific TELu because there are large differences between the proximal and distal lung. Distal lung tissue was excised from the outer edge of the whole lung at a 3 mm distance from the edge. On the contrary, proximal LuOU were generated using the trachea and main

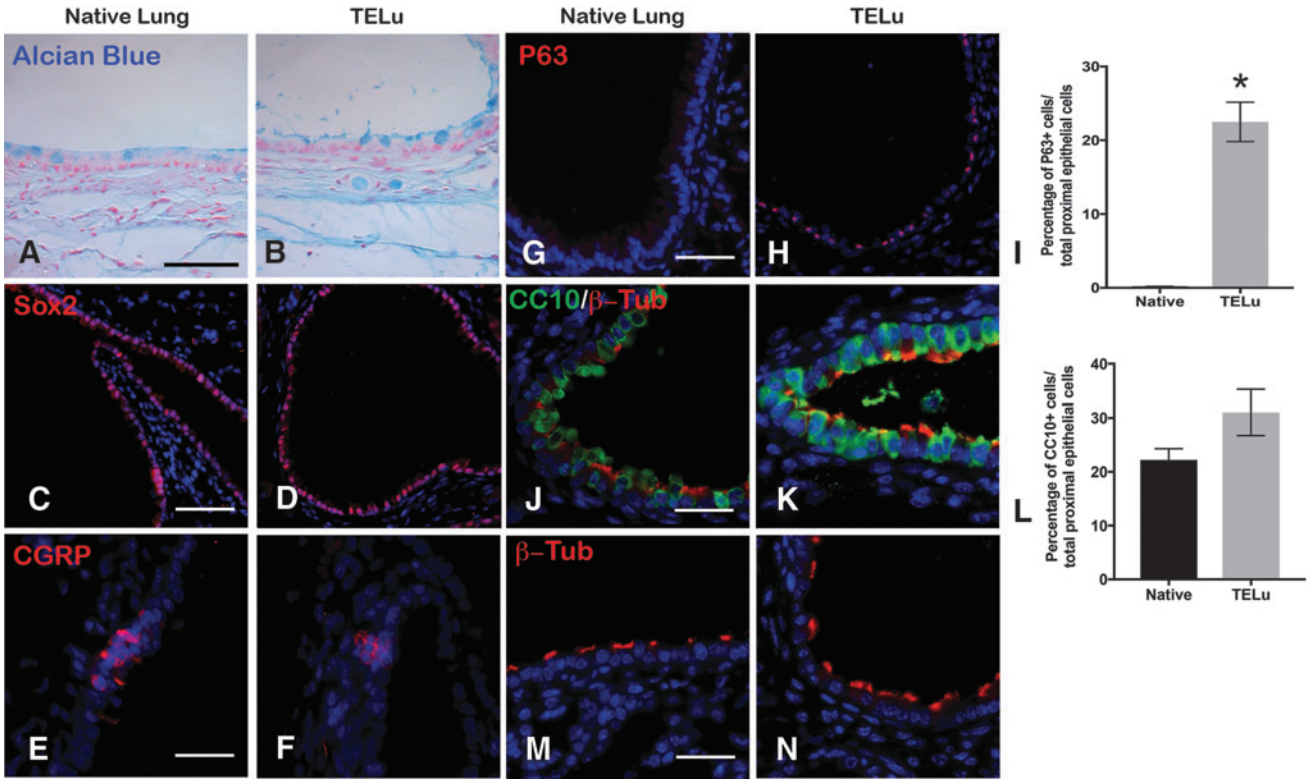


**FIG. 2.** **(A, B)** Alcian blue staining for goblet cells (*blue*) in native airway **(A)** and TELu **(B)**, scale bar 50 μm. **(C, D)** IF for Sox2 (*red*), a marker for proximal airway progenitors, in native lung **(C)** and TELu **(D)**, scale bar 100 μm. **(E, F)** IF for CGRP (*red*), pulmonary neuroendocrine cells in native lung **(E)** and TELu **(F)**, scale bar 50 μm. **(G, H)** IF for p63 (*red*), basal cell marker, **(G)** native airway and **(H)** TELu, scale bar 100 μm. **(I)** Quantification of $p63^{+}$ cells in native lung and TELu. **(J, K)** IF for β-tubulin-IV (*red*), ciliated cells, and CC10 (*green*) in **(J)** native lung and **(K)** TELu, scale bar 50 μm. **(L)** Quantification of percentage of $CC10^{+}$ epithelial cells/total in native lung and TELu. **(M, N)** IF with β-tubulin-IV (*red*) to observe cilia morphology in native lung **(M)** and TELu **(N)**, scale bar 50 μm. $*p = 0.0074$. Color images available online at www.liebertpub.com/tec

stem bronchi. Each of these LuOU preparations was separately seeded onto polymer and transplanted into host animals. TELu generated from distal lung contained AEC1s and AEC2s (Fig. 6A, B). In proximal airway, which we termed TEtrach, numerous epithelial-lined tubular structures were observed on cross section (Fig. 6C, D, K, L). Cartilage was often seen adjacent to the epithelial rings (Fig. 6D), an organization resembling native trachea (Fig. 6C). Ciliated cells lined the TEtrach epithelium (Fig. 6F vs. 6E). Also, CC10-positive club cells were identified in TEtrach similar

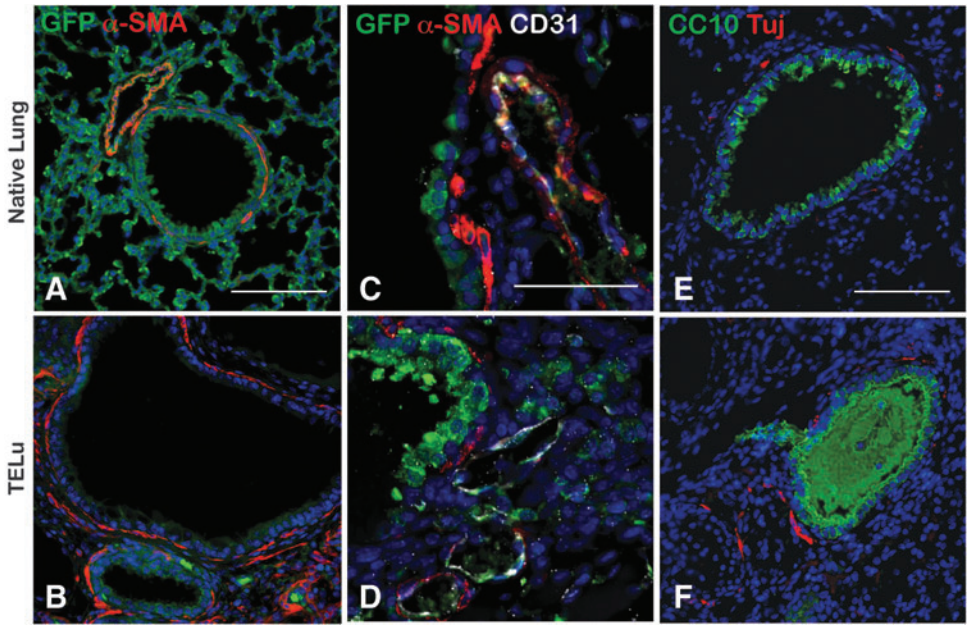


**FIG. 3.** IF staining for mesenchymal structures. **(A, B)** IF for α-SMA (*red*) and GFP (*green*) in $Actin^{GFP}$ native lung **(A)** and $Actin^{GFP}$ TELu **(B)**, scale bar 100 μm. **(C, D)** IF of CD31 (*white*) for endothelial cells, GFP (*green*), and α-SMA (*red*), in $Actin^{GFP}$ native lung **(C)** and $Actin^{GFP}$ TELu **(D)**, scale bar 50 μm. **(E, F)** IF of Tuj (*red*) for ganglia and CC10 (*green*), in native lung **(E)** and TELu **(F)**, scale bar 100 μm. Color images available online at www.liebertpub.com/tec

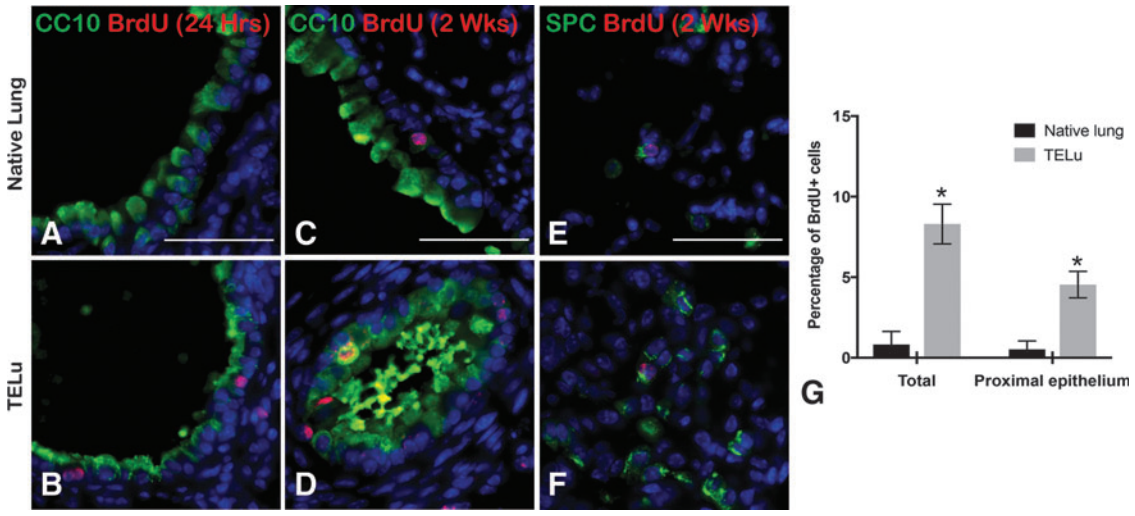


**FIG. 4.** BrdU uptake at 2 and 4 weeks postimplant. **(A, B)** Intraperitoneal BrdU injection 24 h before harvest at 4 weeks postimplant, IF for BrdU (*red*) and CC10 (*green*) in native lung **(A)** and TELu **(B)**. **(C–F)** BrdU injected 2 weeks before harvest at 4 weeks postimplant, IF for BrdU (*red*) and CC10 (*green*) in native lung **(C)** and TELu **(D)**; SPC (*green*) in native lung **(E)** and TELu **(F)**. Quantification of the percentage of $BrdU^+$ cells in native lung versus TELu for total tissue and the proximal epithelium alone **(G)**. Scale bars represent 50 μm. $*p = 0.017$ (total) and $p = 0.034$ (proximal). BrdU, bromodeoxyuridine. Color images available online at www.liebertpub.com/tec

to native trachea (Fig. 6G, H). Basal cells were also identified in TEtrach as shown by p63 staining (Fig. 6J vs. 6I).

Human tissue-engineered trachea (hTEtrach) forms epithelial-lined tubular structures. LuOU were generated from a single $3 \times 4$ mm planar piece of deidentified human trachea obtained during performance of tracheostomy and implanted as described above to obtain hTEtrach. Human tracheal epithelium was noted to have formed in the hTEtrach (Fig. 7A, B). Smooth muscle encircled the tracheal epithelium (Fig. 7C, D). Human basal cells were noted in hTEtrach (Fig. 7E, F). Human tracheal epithelial cell proliferation was identified in hTEtrach epithelium and mesenchyme by Ki67 staining (Fig. 7G, H). Human anti-mitochondrial antibody staining confirmed human donor origin of the hTEtrach (Fig. 7I, J).

## Discussion

Unlike the intestine, the lung is relatively quiescent and, in an uninjured state, has low cellular turnover. Knowledge is still being gained about the regenerative mechanisms of various regions of the lung and airway.[15] In this study, we established a reproducible *in vivo* model of lung regeneration that recapitulated important elements of both mouse and human lungs and key components of both the proximal and distal lung regions. When LuOU were generated from whole lung, TELu contained all key epithelial and mesenchymal cell types, and the origin of the cells was traced from both $Actin^{GFP}$ and $SPC^{GFP}$ donors to indicate that the cells in TELu derived from the transplanted LuOU. Cells, including AEC2s, club cells interspersed with ciliated cells,

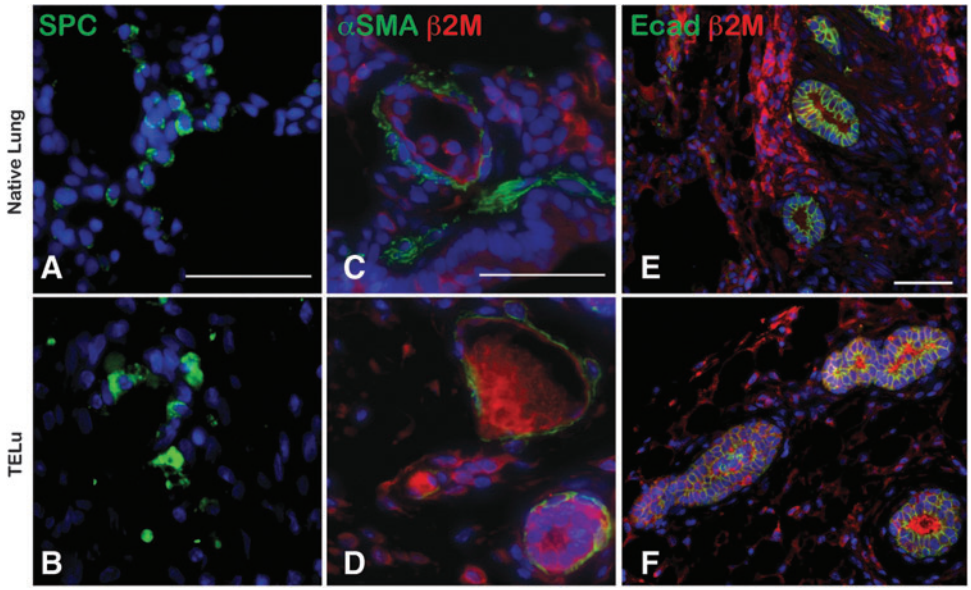


**FIG. 5.** **(A, B)** IF for SPC (*green*) in human lung **(A)** and hTELu **(B)**. **(C, D)** IF for α-SMA (*green*) and human-specific antibody β-2-microglobulin (*red*) in human lung **(C)** and hTELu **(D)**. **(E, F)** IF for E-cadherin (*green*) and β-2-microglobulin (*red*) in human lung **(E)** and hTELu **(F)**. Scale bars 50 μm. hTELu, human TELu. Color images available online at www.liebertpub.com/tec

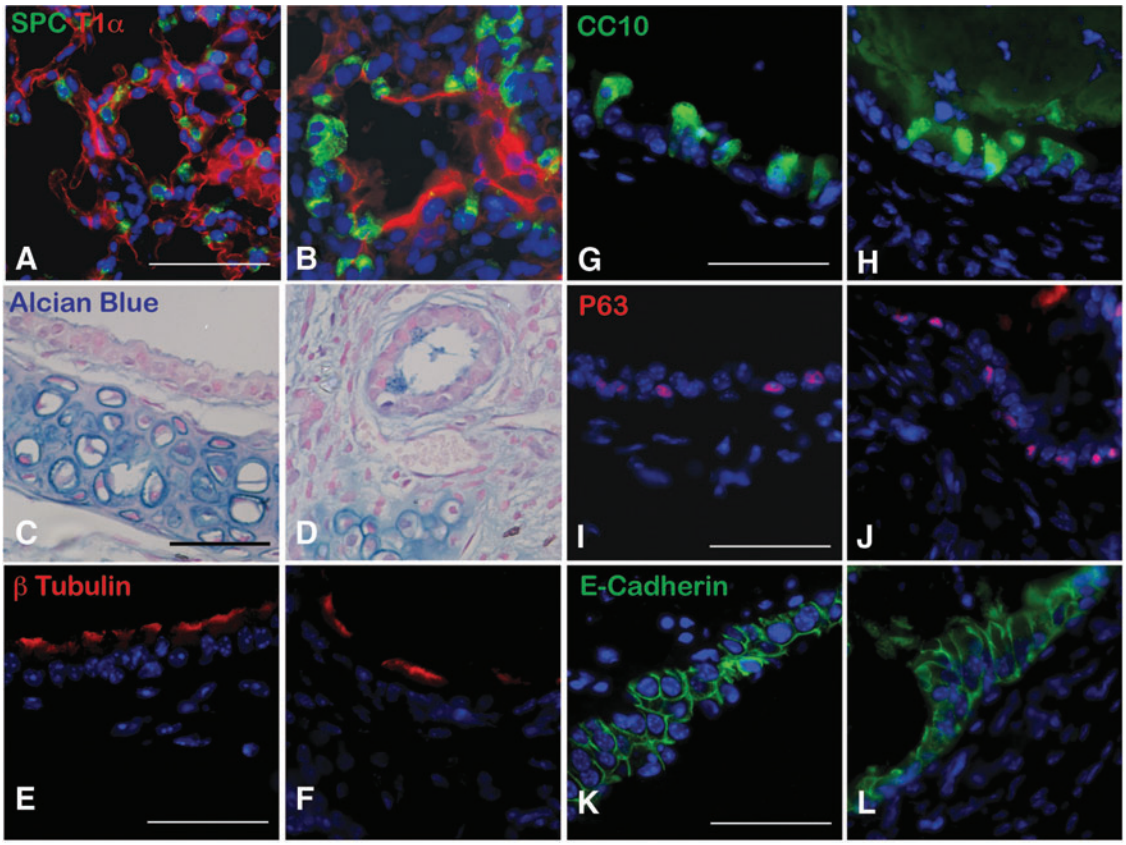


**FIG. 6.** **(A, B)** IF for T1α (*red*) and SPC (*green*) in native lung **(A)** and TELu **(B)** generated from distal LuOU. **(C, D)** Alcian blue stain of native trachea **(C)** and TEtrach generated from proximal airway/tracheal organoid units (proximal LuOU) **(D)**. **(E, F)** IF for β-tubulin-IV (*red*) in native trachea **(E)** and TEtrach **(F)**. **(G, H)** IF for CC10 (*green*) in native trachea **(G)** and TEtrach **(H)**. **(I, J)** IF for p63 (*red*) in native trachea **(I)** and TEtrach **(J)**. **(K, L)** IF for E-Cadherin (*green*) in native trachea **(K)** and TEtrach **(L)**. Scale bars 50 μm. TEtrach, tissue-engineered trachea. Color images available online at www.liebertpub.com/tec

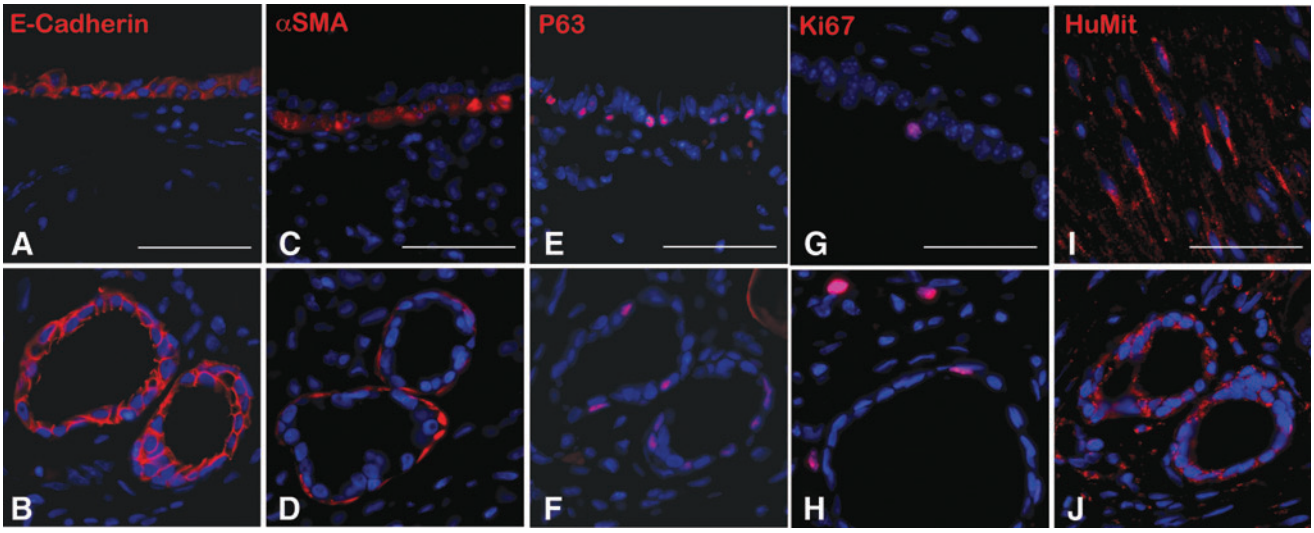


**FIG. 7.** **(A, B)** IF for E-Cadherin (*red*) in native murine trachea **(A)** and hTEtrach **(B)**. **(C, D)** IF for α-SMA (*red*) in native trachea **(C)** and hTEtrach **(D)**. **(E, F)** IF for p63 (*red*) in native trachea **(E)** and hTEtrach **(F)**. **(G, H)** IF for Ki67 (*red*) in native trachea **(G)** and hTEtrach **(H)**. **(I, J)** IF for anti-human mitochondrial antibody (*red*) in positive control human smooth muscle **(I)** and hTEtrach **(J)**. Scale bars 50 μm. hTEtrach, human tissue-engineered trachea. Color images available online at www.liebertpub.com/tec

AEC1s, Sox-2-positive proximal airway progenitors, basal cells, and pulmonary neuroendocrine cells, were also identified in TELu. Low-powered views show the range of structures that are generated from whole lung compared to proximal airway alone, indicating that regional stem/progenitor cell types survive and proliferate. In future work, this may allow lineage tracing of various cell populations to better understand lung regeneration.

The mesenchymal components of peribronchial smooth muscle and nerve were identified with a CD31-positive donor endothelial cell contribution to TELu vasculature. TELu could also be generated from human postnatal tissue as confirmed by human-specific staining of the TELu. Regionally specifying the donor tissue resulted in more specific and limited compositions of the TELu generated from LuOU deriving from proximal tissue originating from either mouse or human. The formation of tubular epithelial structures in TEtrach generated from a human tracheostomy specimen suggests the ability of these progenitor cells to polarize and orient themselves in tubular structures. This is consistent with what we have previously reported for intestinal epithelium.[8,9,11,16,17]

This model includes the known cell types of the proximal and distal respiratory epithelium as well as critical mesenchymal structures. Both are proliferative according to the quantification of BrdU injected 24 h before harvest at 4 weeks. This model results in human lung and tracheal tissue composed of both epithelial and mesenchymal cell types growing from adult progenitor cells derived from human postnatal donors. In other organoid approaches, various components of airway and lung epithelium have been formed *in vitro* and *in vivo*, for example, by purifying populations of $CD31^{-}CD45^{-}EpCAM^{+}Sca1^{+}$ cells cocultured with mouse lung endothelial cells.[18] However, this approach to forming TELu permits growth from postnatally derived multicellular clusters, without sorting steps that may result in cell loss, and maintains key mesenchymal features. In comparison to alternate models in which human embryonic lung tissue has been grown *in vivo* on scaffolds[19] or decellularized scaffolds have permitted temporary survival of isolated cells,[7,20] the subcutaneous implantation site provides ease of construct monitoring and gradual angio-and vasculogenesis that matches the cell growth of the TELu. This avoids the difficulty of reestablishing a complete endothelium in a decellularized graft, which can result in a thrombogenic surface if endothelialization is incomplete.[21]

As multiple groups have noted in other organ systems, the maintenance of three-dimensional relationships in these implants allows the added complexity of numerous cell types of both epithelial and mesenchymal origin, therefore providing a more realistic milieu of cellular signals involved in lung regeneration compared with simpler systems.

There are important differences between the TELu model and native lung. There is no direct communication with the atmosphere; the structure does not recapitulate the patterned alveolarization present in an aerated lung although the cell types of the alveoli are present. In addition, TELu is more proliferative than native lung. Both BrdU and particularly p63 are increased in TELu compared to native lung. p63-positive cells have been shown to proliferate and travel to regions of alveolar damage after H1N1 influenza infection as distal airway stem cells.[22] No BrdU-positive cells were identified in host lungs at 24 h before harvest, correlating with the known slow cellular turnover in mature lungs.[23] However, TELu demonstrated a higher rate of epithelial proliferation as determined by BrdU uptake when compared with native host lungs at 24 h before harvest. BrdU identification revealed more proliferative cells at weeks 2 and 4, although not at week 1, consistent with our observations in tissue-engineered intestine.[9] These time points are relatively long compared to other reports of work *in vivo* with decellularized scaffolds.[24]

In future work, understanding the mechanisms of inducing proliferation of these cells may assist the search for cells that contribute to the repair and regeneration of a relatively nonproliferative organ, in which repair by the formation of fibrosis can be fatal. In addition, study of the native lung in injury and disease is limited by the tolerance of the organism to inevitable declines in oxygenation and ventilation, but damage can be studied in the hosted TELu without impairing the animal's native lung. Study of the reparative processes of the lung and airways is still required to design and translate future human therapies.

## Acknowledgments

This project has received funding from the European Union's Horizon 2020 research and innovation programme under Grant Agreement No. 668294 (T.C.G.), American Heart Association 13SDG16920101 (D.A.), and the Saban Research Institute (D.A.).

## Disclosure Statement

No competing financial interests exist.

## References

1. Kirkby, S., and Hayes, D., Jr. Pediatric lung transplantation: indications and outcomes. J Thorac Dis **6,** 1024, 2014.
2. WHO. The 10 Leading Causes of Death in the World, 2000 and 2012. WHO, 2014. http://www.who.int/mediacentre/factsheets/fs310/en/
3. NIH National Heart, L., and Blood Institute. Disease Statistics. 2012. http://www.nhlbi.nih.gov/about/documents/factbook/2012/chapter4
4. Sellgren, K.L., Butala, E.J., Gilmour, B.P., Randell, S.H., and Grego, S. A biomimetic multicellular model of the airways using primary human cells. Lab Chip **14,** 3349, 2014.
5. Crane, A.M., Kramer, P., Bui, J.H., Chung, W.J., Li, X.S., Gonzalez-Garay, M.L., Hawkins, F., Liao, W., Mora, D., Choi, S., Wang, J., Sun, H.C., Paschon, D.E., Guschin, D.Y., Gregory, P.D., Kotton, D.N., Holmes, M.C., Sorscher, E.J., and Davis, B.R. Targeted correction and restored function of the CFTR gene in cystic fibrosis induced pluripotent stem cells. Stem Cell Reports **4,** 569, 2015.
6. Dye, B.R., Hill, D.R., Ferguson, M.A., Tsai, Y.H., Nagy, M.S., Dyal, R., Wells, J.M., Mayhew, C.N., Nattiv, R., Klein, O.D., White, E.S., Deutsch, G.H., and Spence, J.R. In vitro generation of human pluripotent stem cell derived lung organoids. Elife **4,** e05098, 2015. DOI: 10.7554/eLife.05098
7. Calle, E.A., Mendez, J.J., Ghaedi, M., Leiby, K.L., Bove, P.F., Herzog, E.L., Sundaram, S., and Niklason, L.E. Fate of distal lung epithelium cultured in a decellularized lung extracellular matrix. Tissue Eng Part A **21,** 1916, 2015.

8. Levin, D.E., Barthel, E.R., Speer, A.L., Sala, F.G., Hou, X., Torashima, Y., and Grikscheit, T.C. Human tissue-engineered small intestine forms from postnatal progenitor cells. J Pediatr Surg **48,** 129, 2013.
9. Sala, F.G., Matthews, J.A., Speer, A.L., Torashima, Y., Barthel, E.R., and Grikscheit, T.C. A multicellular approach forms a significant amount of tissue-engineered small intestine in the mouse. Tissue Eng Part A **17,** 1841, 2011.
10. De Langhe, S.P., Sala, F.G., Del Moral, P.M., Fairbanks, T.J., Yamada, K.M., Warburton, D., Burns, R.C., and Bellusci, S. Dickkopf-1 (DKK1) reveals that fibronectin is a major target of Wnt signaling in branching morphogenesis of the mouse embryonic lung. Dev Biol **277,** 316, 2005.
11. Grant, C.N., Mojica, S.G., Sala, F.G., Hill, J.R., Levin, D.E., Speer, A.L., Barthel, E.R., Shimada, H., Zachos, N.C., and Grikscheit, T.C. Human and mouse tissue-engineered small intestine both demonstrate digestive and absorptive function. Am J Physiol Gastrointest Liver Physiol **308,** G664, 2015.
12. Spurrier, R.G., Speer, A.L., Grant, C.N., Levin, D.E., and Grikscheit, T.C. Vitrification preserves murine and human donor cells for generation of tissue-engineered intestine. J Surg Res **190,** 399, 2014.
13. Singh, G., and Katyal, S.L. An immunologic study of the secretory products of rat Clara cells. J Histochem Cytochem **32,** 49, 1984.
14. Hogan, B.L., Barkauskas, C.E., Chapman, H.A., Epstein, J.A., Jain, R., Hsia, C.C., Niklason, L., Calle, E., Le, A., Randell, S.H., Rock, J., Snitow, M., Krummel, M., Stripp, B.R., Vu, T., White, E.S., Whitsett, J.A., and Morrisey, E.E. Repair and regeneration of the respiratory system: complexity, plasticity, and mechanisms of lung stem cell function. Cell Stem Cell **15,** 123, 2014.
15. Kotton, D.N., and Morrisey, E.E. Lung regeneration: mechanisms, applications and emerging stem cell populations. Nat Med **20,** 822, 2014.
16. Barthel, E.R., Levin, D.E., Speer, A.L., Sala, F.G., Torashima, Y., Hou, X., and Grikscheit, T.C. Human tissue-engineered colon forms from postnatal progenitor cells: an in vivo murine model. Regen Med **7,** 807, 2012.
17. Speer, A.L., Sala, F.G., Matthews, J.A., and Grikscheit, T.C. Murine tissue-engineered stomach demonstrates epithelial differentiation. J Surg Res **171,** 6, 2011.
18. Lee, J.H., Bhang, D.H., Beede, A., Huang, T.L., Stripp, B.R., Bloch, K.D., Wagers, A.J., Tseng, Y.H., Ryeom, S., and Kim, C.F. Lung stem cell differentiation in mice directed by endothelial cells via a BMP4-NFATc1-thrombospondin-1 axis. Cell **156,** 440, 2014.
19. Nakayama, K.H., Lee, C.C., Batchelder, C.A., and Tarantal, A.F. Tissue specificity of decellularized rhesus monkey kidney and lung scaffolds. PLoS One **8,** e64134, 2013.
20. Raredon, M.S., Rocco, K.A., Gheorghe, C.P., Sivarapatna, A., Ghaedi, M., Balestrini, J.L., Raredon, T.L., Calle, E.A., and Niklason, L.E. Biomimetic culture reactor for whole-lung engineering. Biores Open Access **5,** 72, 2016.
21. Stabler, C.T., Lecht, S., Mondrinos, M.J., Goulart, E., Lazarovici, P., and Lelkes, P.I. Revascularization of decellularized lung scaffolds: principles and progress. Am J Physiol Lung Cell Mol Physiol **309,** L1273, 2015.
22. Kumar, P.A., Hu, Y., Yamamoto, Y., Hoe, N.B., Wei, T.S., Mu, D., Sun, Y., Joo, L.S., Dagher, R., Zielonka, E.M., Wang de, Y., Lim, B., Chow, V.T., Crum, C.P., Xian, W., and McKeon, F. Distal airway stem cells yield alveoli in vitro and during lung regeneration following H1N1 influenza infection. Cell **147,** 525, 2011.
23. Boers, J.E., Ambergen, A.W., and Thunnissen, F.B. Number and proliferation of clara cells in normal human airway epithelium. Am J Respir Crit Care Med **159,** 1585, 1999.
24. Ott, H.C., Clippinger, B., Conrad, C., Schuetz, C., Pomerantseva, I., Ikonomou, L., Kotton, D., and Vacanti, J.P. Regeneration and orthotopic transplantation of a bioartificial lung. Nat Med **16,** 927, 2010.

Address correspondence to:
*Tracy C. Grikscheit, MD*
*Division of Pediatric Surgery*
*Children's Hospital Los Angeles*
*4650 Sunset Boulevard, Mailstop No. 100*
*Los Angeles, CA 90027*

*E-mail:* tgrikscheit@chla.usc.edu

*Received: June 29, 2016*
*Accepted: October 28, 2016*
*Online Publication Date: November 14, 2016*